Filling Large Discontinuities in 3D Vascular Networks Using Skeleton- and Intensity-Based Information

Russell Bates[1], Laurent Risser[2], Benjamin Irving[1], Bartłomiej W. Papież[1], Pavitra Kannan[3], Veerle Kersemans[3,⋆], and Julia A. Schnabel[1]

[1] Institute of Biomedical Engineering,
Department of Engineering Science, University of Oxford, UK
[2] Institut de Mathématiques de Toulouse (UMR 5219), CNRS, France
[3] Department of Oncology, University of Oxford, UK

Abstract. Segmentation of vasculature is a common task in many areas of medical imaging, but complex morphology and weak signal often lead to incomplete segmentations. In this paper, we present a new gap filling strategy for 3D vascular networks. The novelty of our approach is to combine both skeleton- and intensity-based information to fill *large* discontinuities. Our approach also does not make any hypothesis on the network topology, which is particularly important for tumour vasculature due to the chaotic arrangement of vessels within tumours. Synthetic results show that using intensity-based information, in addition to skeleton-based information, can make the detection of large discontinuities more robust. Our strategy is also shown to outperform a classic gap filling strategy on 3D Micro-CT images of preclinical tumour models.

1 Introduction

Gap filling methods for vascular networks have recently generated significant interest. Many methods for the segmentation of the vasculature rely on the generation of a likelihood or *vesselness* map. To obtain a final segmentation, these maps are usually binarized, meaning that important vessel information may be discarded. Under-segmentation in this sense can lead to discontinuities in the segmentation, which will have implications for any analysis of the branching structure. In this paper, we then propose a novel method to incorporate image intensity information, additional to the final segmentation, to reconnect the gaps in the segmentation. This method is motivated by the extraction of tumour vasculature which is highly leaky and poorly perfused, leading to an irregular distribution of signal within the vasculature (see Fig. 1). No strong hypotheses can therefore be made on their chaotic and highly irregular topology.

⋆ We would like to acknowledge funding from the CRUK/ EPSRC Cancer Imaging Centre in Oxford. JAS and LR also wish to acknowledge the CNRS-INSMI/John Fell Oxford University Press (OUP) Research Fund.

N. Navab et al. (Eds.): MICCAI 2015, Part III, LNCS 9351, pp. 157–164, 2015.
DOI: 10.1007/978-3-319-24574-4_19

Preliminary approaches to perform gap filling or to improve robustness in the segmentation of vascular structures were proposed in [10,13,9]. A gap filling strategy for large 3D images with a discontinuous segmented vasculature, based on a tensor voting strategy [4], was proposed in [11]. This approach, however, only makes use of the skeleton of segmented structures. Another tensor voting strategy was proposed in [7] to segment noisy tubular structures in an iterative fashion. However, this only applies to relatively small gaps. An interesting learning strategy was proposed in [5]. This approach utilizes human interactions to learn appropriate graph connectivity. The decomposition of directional information, *orientation scores*, has been explored [2], but with application to crossing vessels. This high level strategy is complementary to lower level ones like in [11], where only local image features communicate to fill the gaps. In the same vein, the simultaneous reconstruction and separation of multiple interwoven tree structures using high-level representation of the trees was also proposed in [1], and a physiologically motivated strategy based on a simplified angiogenesis model was proposed in [12] to correct the vascular connectivity. Closer to our strategy, [3] derived intensity based information within a tensor model to perform the robust segmentation of tubular structures. However, this strategy is dedicated to robust vessel segmentation in a noisy context, which would typically lead to small discontinuities, and not to the detection of large discontinuities in the segmented network. Note finally that a review of 3D vessels segmentation strategies was recently published in [6].

From a methodological perspective, we define a gap filling strategy adapted to *large discontinuities*. Our approach works on very low level features and places few priors on the structure, distribution and topology of the vessels. Its key novelties are (1) the incorporation of both skeletal and image intensity information whilst enforcing minimal priors on the resultant reconnected morphology, and (2) a new communication model between the different image features, with the clear separation of oriented- and non oriented-information. This paper is structured as follows: Section 2 presents our new gap filling strategy. Results are presented section 3 and discussions are drawn section 4.

2 Methodology

2.1 Method Overview

Suppose we have the following inputs defined on the image domain Ω:

1. A skeletonized vascular network, typically obtained from a segmented vascular network. We denote s_i, $i \in \{1, \cdots, I\}$ the set of network *segments* which contain the set of points between two topological branch points or between a branch point and an end point. The $\mathbf{e}_j$, $j \in \{1, \cdots, J\}$ are the set of *segment ends* connected to any other segment.
2. A list of *uncertain points* $\mathbf{p}_k$, $k \in \{1, \cdots, K\}$ and their intensity w_k, $w_k \in [0, 1]$. Intensities are normalized so that w_k close to 0 means that point $\mathbf{p}_k$ is unlikely to be part of a vessel and w_k close to 1 means that $\mathbf{p}_k$ is very likely

to be part of a vessel. These intensities can be directly extracted from the original image or as the scores of a probabilistic segmentation algorithm.

Fig. 1 illustrates these image features. From each segment end $\mathbf{e}_j$, a path P_j will eventually be generated to fill a gap in the skeleton. To do so, the user has only to define two simple parameters:

1. Characteristic distance σ which represents the typical size of the gaps to fill.
2. Characteristic angle $\theta \in]0, \pi/2[$ of the paths, which permits more or less curvature to an optimal path. A typical value for θ is $\pi/5$.

Based on the segment ends $\mathbf{e}_j$, our strategy first consists of defining a second order tensor field $\mathbf{T}$. This field is used to compute the saliency map to curvilinear shapes S as in [11], plus preferential directions $\mathbf{D}$ for the path search. Based on the segments s_i and intensity based information ($\mathbf{p}_k$,w_k), a so-called enhancement map E is generated to indicate where each path P_j could be found without any clear indication on its local orientation. This differs from [11], where all input information is expressed in the tensor field with preferential directions. Note that we build the two scalar fields S and E so that, for both of them, a value close to 0 at point $\mathbf{p}$ emphasizes that $\mathbf{p}$ should not be part of a path P_j, and values similar to or larger than 1 emphasize that $\mathbf{p}$ is very likely to be part of a path P_j. We describe hereafter how paths P_j are generated using the fields S, E and $\mathbf{D}$. Construction of these fields is described in the following.

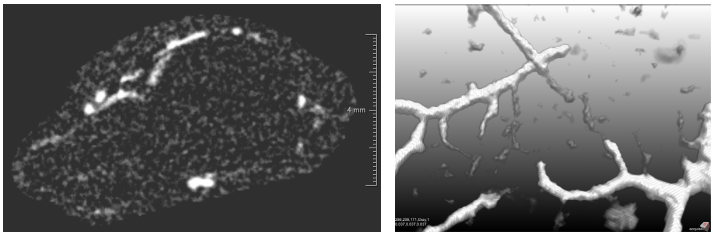

Fig. 1. **(left)** Slice out of a 3D image of tumour vasculature. **(right)** Primary 3D segmentation shown in white and intensity information shown in gray. In our model, the primary segmentation is skeletonized and intensity information provides an additional guide for reconnection. In the presented ROI, this additional information makes sense to fill skeleton discontinuities.

2.2 Gap Filling

The segment ends $\mathbf{e}_j$ can be linked to other segment ends in case of a gap within a vessel segment, or to other segments s_i in case of a gap at a bifurcation. We use Alg. 1 to generate the paths. Parameter δ is the step length of the

recursive path search and is typically similar to the voxel resolution. We define h as equal to 0.05. This is motivated by the fact that the effect of this threshold is largely redundant with respect to σ and θ. Angles θ_1 and θ_2 also ensure that the path search is relatively smooth and follows directions similar to the preferential directions of $\mathbf{D}$. We consider these parameters as secondary here and set them to 20 degrees. However, our tests have shown that they should be contained within $[10, 30]$ degrees to lead to satisfactory results, whatever the network. Note that our algorithm was chosen over a Dijkstra style search algorithm for reasons of computational complexity.

Algorithm 1. Path search from a segment end e_j

1: $P_j(1) = \text{location}(\mathbf{e}_j)$
2: $P_j(2) = \text{location}(\mathbf{e}_j) + \delta\text{direction}(\mathbf{e}_j)$
3: $i = 2$
4: **while** [$P_j(i)$ does not reach a segment end or a segment] and [$\max(S(P_j(i)), E(P_j(i))) > h$] **do**
5: List all points $\hat{P}_j(i+1)$ at a distance δ from $P_j(i)$
6: Among the $\hat{P}_j(i+1)$, remove those for which the angle between $P_j(i-1)P_j(i)$ and $P_j(i)\hat{P}_j(i+1)$ is higher than θ_1.
7: Among the $\hat{P}_j(i+1)$, remove those for which the angle between $\mathbf{D}(P_j(i))$ and $P_j(i)\hat{P}_j(i+1)$ is higher than than θ_2.
8: If there remains at least one point in the list $P_j(i+1)$ is the one which have the highest $\max(S(P_j(i)), E(P_j(i)))$
9: i++
10: **end while**
11: If $P_j(i)$ reaches a segment end or a segment, then join $\mathbf{e}_j$ with this token using P_j
end

2.3 Generating the Second-Order Tensor Field T

A second-order tensor field constructed from the dyadic products of a vector field allows for a simple mechanism of communication between vector fields. We use a very similar technique as in [11] to define the tensor field $\mathbf{T}$. Let l_j be the location of the segment end $\mathbf{e}_j$ and $\mathbf{d}_j$ be its (normalized) direction. For each point $\mathbf{p}$ close to l_j, a vector $\mathbf{w}_j(p)$ is first generated as:

$$\mathbf{w}_j(\mathbf{p}) = e^{\frac{r^2 + c\varphi^2}{\sigma^2}} (2\mathbf{e}_j\mathbf{p}(\mathbf{e}_j\mathbf{p} \cdot \mathbf{d}_j) - \mathbf{d}_j) \,, \tag{1}$$

where c equals $\sigma^3/(4\sin^2\theta)$ and $(\mathbf{e}_j\mathbf{p} \cdot \mathbf{d}_j)$ is the scalar product between $\mathbf{e}_j\mathbf{p}$ and $\mathbf{d}_j$. Scalars r and φ are, respectively, the length and the curvature of an arc of circle going through $\mathbf{e}_j$ and $\mathbf{p}$ and parallel to $\mathbf{d}_j$ at point $\mathbf{e}_j$ (as in [11]). At each point $\mathbf{p}$, the communication between all segment ends is simply performed by computing the sum of all *tensorized* vector fields $\mathbf{w_j}$:

$$\mathbf{T}(\mathbf{p}) = \sum_{j=1}^{J} \mathbf{w}_j(\mathbf{p}) \otimes \mathbf{w}_j(\mathbf{p}) \,, \tag{2}$$

where $\otimes$ is the tensor product between two vectors. This strategy will allow us to evaluate whether all vectors $\mathbf{w}_j(\mathbf{p})$ have similar directions, by computing the eigenvalues and eigenvectors of $\mathbf{T}(\mathbf{p})$.

2.4 Deriving a Saliency Map S and Preferential Directions D from T

Our method works on the hypothesis that segments are connected when both ends agree on some path between them. The saliency map is a measure for this agreement by quantifying the degree to which votes from different segments at a given point agree on a preferential direction. As in [4,11,7], each point of $\mathbf{T}$ can be decomposed into eigenvectors and eigenvalues, which describe the principal directions of $\mathbf{T}$ and their strength at each point p: $\mathbf{T}(\mathbf{p}) = \sum_{i=1}^{3} \sigma_i(\mathbf{p})\mathbf{v}_i(\mathbf{p}) \otimes \mathbf{v}_i(\mathbf{p})$. Decomposition can be performed using the Jacobi algorithm. The saliency to a curvilinear shape $S(\mathbf{p})$, defining how likely each point of the domain is to be part of a curve, is defined by $S(\mathbf{p}) = \sigma_1(\mathbf{p}) - \sigma_2(\mathbf{p})$. As the weights given to each vector field $\mathbf{w}_j(\mathbf{p})$ expressing a single segment end in Eq. (1) are contained between 0 and 1, we assume that $S(\mathbf{p})$ higher than 1 means that the saliency of $\mathbf{p}$ to a curve is very high.

Preferential directions $\mathbf{D}$ to join two segment ends can simply be the eigenvector $\mathbf{v}_1$ corresponding to the largest eigenvalue. Note that these eigenvectors are defined on a larger domain than where $S(\mathbf{p}) > h$, which will be the key for the use of the enhancement field E.

2.5 Generating the Enhancement Map E

We first enhance segment surroundings in E: at a point $\mathbf{p}$ close to a segment s_i, we set $E(\mathbf{p}) = \exp\left(-4c^2/\sigma^2\right)$, where c is the distance between $\mathbf{p}$ and s_i.

Then, in order to estimate how uncertain points $\mathbf{p}_k$ and their intensities w_k are expressed in E, we first copy them in a temporary image R_1. All other points of R_1 are null. We then define the temporary images R_2 and R_3 by smoothing R_1 with a kernel $\exp\left(-4d^2/\sigma^2\right)$ and a larger kernel $\exp\left(-d^2/\sigma^2\right)$ respectively, where d is the distance to the kernel origin. Each point $\mathbf{p}$ of E is then influenced by the uncertain points $E(\mathbf{p}) = E(\mathbf{p}) + R_2(\mathbf{p})/R_3(\mathbf{p})$. This approach ensures that a locally isolated point $\mathbf{p}_k$ or a local cluster of uncertain points with the same intensities w_k will be similarly spread in R_2/R_3 (close to Gaussian smoothing) with a maximum value of w_k. As the intensities are sampled within $[0, 1]$, the influence of isolated uncertain points or groups of uncertain points is then similar to the influence of the segments s_i in E and the influence of the segment ends $\mathbf{e}_j$ in S. All non-oriented information for the path search is then sampled on the same scale, which facilitates the communication between skeleton- and intensity-based information in the path search of section 2.2.

3 Results

3.1 Synthetic Data

A synthetic example and two sets of results are presented in Fig. 2. Although this network has no physiological meaning, it represents different configurations which may occur in our application: (top) two segment ends, one in front of the other; (left) segment end pointing a segment; (bottom-right) two segment ends which are relatively close to a segment but with intensity based information indicating that they should be linked together and not linked to the segment. The two first cases can be easily merged using skeleton information only (right illustrations of Fig. 2) but the third one requires intensity information (central illustrations of Fig. 2). A comparison with [11] also led to the same results as our strategy without intensity information. Using large values of σ a false positive junction would be made. Using reasonable σ, as well as intensity information, the two segment ends are properly merged (illustrations on the central column of Fig. 2).

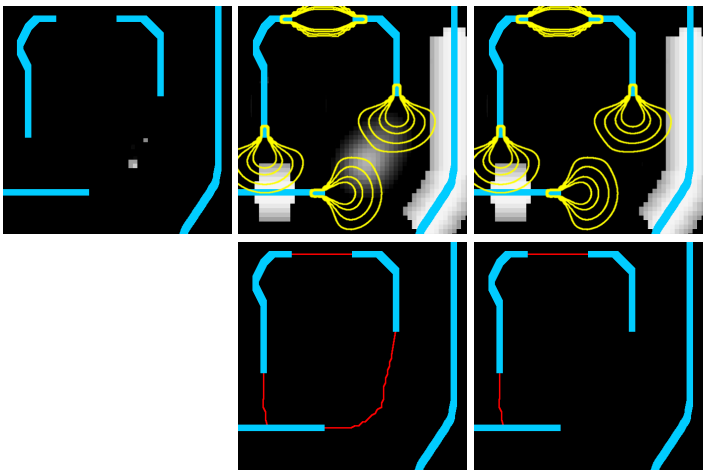

Fig. 2. Gap filling in a synthetic 2D network. Large blue curves represent the initial skeleton. Gray levels represent initial intensities in the top-left image and the enhancement field E in other images. They are sampled between 0 and 1. Yellow curves are the isolines [0.3, 0.2, 0.1, 0.05] of the saliency map S. Thin red curves are the paths P_j filling discontinuities.

3.2 3D Images of Tumour Vasculature

10 volumes of a preclinical tumour model were acquired using the CT component of an Inveon PET/CT system (Siemens Healthcare) with an isotropic voxel size of 32.7μm on a 300×200×170 grid size. The images were derived from a female CBA mouse with murine adenocarcinoma NT (CaNT) implanted subcutaneously on the right flank. For contrast enhanced micro-CT scanning, the

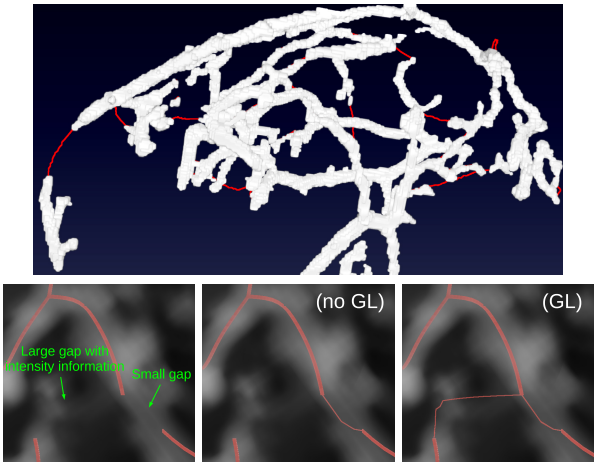

Fig. 3. Result obtained on a 3D tumour vasculature using the proposed strategy. **(Top)** Segmented network is in white and the red curves are the paths P_j filling discontinuities. **(Bottom)** ROI in which intensity information made it possible to fill a gap.

contrast agent Exitron^{TM} nano 12000 (Miltenyi Biotec) was injected into the lateral tail vein and segmentations were performed on the subtraction of pre- and post-contrast agent scans with a vesselness measure derived from [14]. Our primary segmentation was performed using a Markov Random Field approach which leads to a largely contiguous segmentation. The skeletonization algorithm of [8] was used on this segmentation. The secondary segmentation, from which the guiding intensity values were drawn, was formed from a simple thresholding operation which is slightly more permissive than the MRF technique. We compared our strategy to [11], which does not make use of intensity-based information and uses a different communication strategy between the different skeleton elements. We tested our model with (referred by (GL)) and without (referred by (no GL)) intensity information to measure its benefit. The same gap filling parameters were used for all methods ($\sigma = 400\mu$m and $\theta = 25$ degrees).

In total 60 gaps were filled using [11] whereas 75 and 95 gaps were filled using strategies (no GL) and (GL) respectively. None of them are obvious false positives.

4 Discussion

We have presented a new gap filling model using skeleton- and intensity-based information simultaneously, which separates non-oriented (in E and S) and oriented (in $\mathbf{D}$) communication between the different skeleton elements. Here, the oriented information $\mathbf{D}$ is only derived from the segment ends and gives soft preferential directions to fill the gaps. Therefore, it prevents unrealistic junctions.

Saliency to curvilinear structures S is only considered in a reasonable neighborhood around the segment ends, as it may make little sense at a large distance. Finally, the enhancement maps E can help to perform long distance connections with the soft constrains given by $\mathbf{D}$. In our results, obtained on real 3D tumour vasulature, the use of E in addition to S allowed us to fill additional large gaps and did not generate obvious false positive junctions. We believe this to be an encouraging result.

References

1. Bauer, C., Pock, T., Sorantin, E., Bischof, H., Beichel, R.: Segmentation of interwoven 3d tubular tree structures utilizing shape priors and graph cuts. Medical Image Analysis 14, 172–184 (2010)
2. Bekkers, E., Duits, R., Berendschot, T., ter Haar Romeny, B.: A Multi-Orientation Analysis Approach to Retinal Vessel Tracking. J. Math. Imaging and Vision 49, 583–610 (2014)
3. Cetin, S., Demir, A., Yezzi, A.J., Degertekin, M., Ünal, G.B.: Vessel Tractography Using an Intensity Based Tensor Model With Branch Detection. IEEE Trans. Med. Imaging 32, 348–363 (2013)
4. Guy, G., Medioni, G.: Inference of surfaces, 3-D curves, and junctions from sparse, noisy, 3-D data. IEEE Trans. Pat. Anal. Mach. Int. 26, 1265–1277 (1997)
5. Kaufhold, J.P., Tsai, P.S., Blinder, P., Kleinfeld, D.: Vectorization of optically sectioned brain microvasculature: Learning aids completion of vascular graphs by connecting gaps and deleting open-ended segments. Medical Image Analysis 16, 1241–1258 (2012)
6. Lesage, D., Angelini, E.D., Bloch, I., Funka-Lea, G.: A review of 3D vessel lumen segmentation techniques: Models, features and extraction schemes. Medical Image Analysis 13, 819–845 (2009)
7. Loss, L.A., Bebis, G., Parvin, B.: Iterative Tensor Voting for Perceptual Grouping of Ill-Defined Curvilinear Structures. IEEE Trans. Med. Imaging 30, 1503–1513 (2011)
8. Palágyi, K., Kuba, A.: A 3-D 6-subiteration thinning algorithm for extracting medial lines. Pattern Recogn. Lett. 19, 613–627 (1998)
9. Pock, T., Janko, C., Beichel, R., Bischof, H.: Multiscale medialness for robust segmentation of 3-d tubular structures. In: Proc. CVW Workshop (2005)
10. Quek, F.K.H., Kirbas, C.: Vessel extraction in medical images by wave-propagation and traceback. IEEE Trans. Med. Imaging 20, 117–131 (2001)
11. Risser, L., Plouraboué, F., Descombes, X.: Gap Filling in Vessel Networks by Skeletonization and Tensor Voting. IEEE Trans. Med. Imaging 27, 674–687 (2008)
12. Schneider, M., Hirsch, S., Weber, B., Székely, G., Menze, B.H.: TGIF: Topological Gap In-Fill for Vascular Networks. In: Golland, P., Hata, N., Barillot, C., Hornegger, J., Howe, R. (eds.) MICCAI 2014, Part II. LNCS, vol. 8674, pp. 89–96. Springer, Heidelberg (2014)
13. Szymczak, A., Tannenbaum, A., Mischaikow, K.: Coronary vessel cores from 3-d imagery: A topological approach. In: Proc. SPIE Med. Imag. (2005)
14. Xiao, C., Staring, M., Shamonin, D., Reiber, J.H., Stolk, J., Stoel, B.C.: A strain energy filter for 3D vessel enhancement with application to pulmonary CT images. Medical Image Analysis 15, 112–124 (2011)